Next-To-Leading Order QCD Corrections to Associated Production of a SM Higgs Boson with a Pair of Weak Bosons in the POWHEG-BOX

Julien Baglio*

Institut für Theoretische Physik, Eberhard Karls Universität Tübingen, Auf der Morgenstelle 14, D-72076 Tübingen, Germany

(Dated: February 17, 2016)

After the discovery of a Higgs boson in 2012 at the CERN Large Hadron Collider (LHC) the detailed study of its properties, and most importantly its couplings to other particles, has started. This is a very important task to be completed, in particular to test whether it is indeed the Higgs boson predicted by the Standard Model (SM). The precise study of the Higgs couplings to gauge bosons is of particular importance and requires as much information as possible. In this view this paper provides the next-to-leading order (NLO) QCD corrections to the production cross sections and differential distributions of a SM Higgs boson in association with a pair of weak bosons W^+W^-, $W^\pm Z$ and ZZ, matched with parton shower (PS) in the POWHEG-BOX framework. The NLO QCD corrections are found to be significant and PS effects are sizable at low p_T in the jet differential distributions, as expected, while these effects are negligible in other distributions. We will also provide a detailed study of the theoretical uncertainties affecting the total production rates at the LHC and at the Future Circular Collider in hadron-hadron mode, the potential 100 TeV follow-up of the LHC machine: the scale uncertainty calculated by the variation of the renormalization and factorization scales, the parton distribution function and related α_s errors as well as the parametric uncertainties on the input weak boson masses.

PACS numbers: 12.38.Bx,14.70.Fm,14.70.Hp,14.80.Bn

arXiv:1512.05787v2 [hep-ph] 16 Feb 2016

I. INTRODUCTION

The discovery of a Higgs boson with a mass of around 125 GeV is the big highlight of Run I of the Large Hadron Collider (LHC) at CERN [1, 2]. The Higgs boson is the remnant of the electroweak symmetry-breaking (EWSB) mechanism [3–6] that gives the masses to the other fundamental particles and unitarizes the scattering of weak bosons. Since the discovery the measured signal strengths have agreed with the expectations from the Standard Model (SM) [7–9] even if the experimental uncertainties still leave (a small) room for more exotic scenarios [10, 11]. In order to pin down the potential new physics aspects it is then of utmost importance to develop the most exhaustive survey of the possible production channels and decay branching fractions for the Higgs boson in the SM to further add to the Higgs coupling measurements. In this view the production of a Higgs boson in association with a pair of weak gauge bosons [12–15] can be used to probe the Higgs gauge couplings [16] that is also directly related to the triple gauge boson vertex [17]. Given the size of the production cross sections the measurement of this associated production will be of interest not for the LHC Run II, but for the high-luminosity LHC and the Future Circular Collider in hadron-hadron mode (FCC-hh) [18], the potential machine that would follow the LHC with an energy of 100 TeV. In particular the channel $pp \to HW^+W^- \to b\bar{b}W^+W^-$ has a cross section at the 14 TeV LHC that is 50% larger than the corresponding cross section for the HH channel $pp \to HH \to b\bar{b}W^+W^-$, the latter being already considered by the LHC experiments for the high-luminosity LHC run [19]. This leaves room for further phenomenological studies for the associated production of a Higgs boson with a pair of weak bosons.

In the past few years the calculation of the next-to-leading order (NLO) QCD corrections to various SM $H + VV'$ processes at the LHC have been completed: HW^+W^- production [20], $HW^\pm Z$ production [21] and the associated production with a massive gauge boson W/Z and a photon [22, 23]. The calculation of the NLO corrections to the HZZ production cross section is still missing. The purpose of this paper is not only to fill this gap by calculating the NLO QCD corrections to HZZ production but also to provide for the production channels involving massive weak bosons, for the first time, the matching with parton shower (PS) in the `POWHEG-BOX` framework [24, 25]. It will be shown that the hierarchy $WW : WZ : ZZ$ (with ratio 7:3:1) observed in the production of pairs of massive weak bosons [26] remains in the associated production of these pairs with a Higgs boson, albeit with the different ratio 4:2:1. One particular difference is the hierarchy between the HW^+Z and HZZ cross sections that is inverted at low center-of-mass (c.m.) energies compared to the hierarchy between the W^+Z and ZZ channels.

The detailed study of the theoretical uncertainties affecting the calculation of the total cross sections is also presented both for the LHC and the FCC-hh. These uncertainties include the scale uncertainty stemming from the variation of the renormalization and the factorization

* julien.baglio@uni-tuebingen.de

scales; the uncertainty related to the parton distribution function (PDF) and the associated error on the determination of the strong coupling constant α_s. The uncertainties related to the experimental errors on the W and Z masses are found to be negligible.

This paper is organized as follows. In Section II the details of the calculational method are presented for the three production channels. Section III presents the numerical results for the differential distributions and the discussion of the impact of PS effects. Section IV is devoted to the study of the total rates at the LHC and at the FCC-hh including the theoretical uncertainties. A short conclusion is given in Section V.

II. DETAILS OF THE CALCULATION

A. Leading Order $q\bar{q}' \to HVV'$ Partonic Subprocesses

In this paper the production of on-shell massive weak bosons in association with a SM Higgs boson at a proton-proton collider is considered. The contributions from the third-generation quarks in the initial state are excluded, nevertheless the running of the strong coupling constant α_s will be done with five active massless flavors. The calculation is done in the 't Hooft-Feynman gauge. The main mechanisms to produce a pair of weak bosons in association with a Higgs boson at leading order (LO) proceed via quark-antiquark annihilations and are depicted in Fig. 1. In the case of HW^+W^- and HZZ processes we have at partonic level

$$q + \bar{q} \to HW^+W^-, HZZ \quad (q = u, d, s, c), \tag{1}$$

where only diagonal Cabibbo-Kobayashi-Maskawa (CKM) matrix elements are used for HW^+W^- process as the nondiagonal corrections are negligible. In the case of $HW^\pm Z$ processes we have this time all possible CKM combinations with four flavors,

$$q + \bar{q}' \to HW^\pm Z \quad (q\bar{q}' = u\bar{d}, u\bar{s}, c\bar{d}, c\bar{s}; d\bar{u}, s\bar{u}, d\bar{c}, s\bar{c}). \tag{2}$$

Diagrams involving a Yukawa coupling between a light quark and a Higgs boson are discarded. The LO hadronic cross section is defined as

$$\sigma_{\rm LO} = \int \mathrm{d}x_1 \mathrm{d}x_2 [q_{\rm LO}(x_1, \mu_F) \bar{q}'_{\rm LO}(x_2, \mu_F) \hat{\sigma}^{q\bar{q}' \to HVV'}_{\rm LO} + (1 \leftrightarrow 2)], \tag{3}$$

where q and $\bar{q}'$ are the PDFs of the first- and second-generation quarks in the proton at the momentum fraction x and factorization scale μ_F, and $\hat{\sigma}^{q\bar{q}' \to HVV'}$ is the LO partonic cross section.

In the following we will describe the method and the tools used for the calculation of the NLO QCD corrections. We want to stress at this point that two types of higher-order corrections for the HW^+W^- process have been studied in the literature: the NLO QCD corrections for the quark-antiquark annihilation processes and the one-loop gluon fusion contribution $gg \to HW^+W^-$, the latter leading to a correction of $+4.5\%$ at $M_H = 120$ GeV [20]. Together with the corresponding contribution for the HZZ channel that is still yet to be calculated, $gg \to HZZ$, these gluon fusion contributions are α_s^2-order corrections and thus next-to-next-to-leading order (NNLO) contributions to the whole hadronic processes. We do not include this type of contributions in this paper as we want to do a consistent analysis at NLO QCD including PS effects. Including these NNLO corrections requires a careful matching in the differential distributions that is left to be studied in a future paper.

B. NLO $q\bar{q}' \to HVV' + X$ Corrections

The NLO QCD corrections to the quark-antiquark annihilation partonic processes proceed via virtual one-loop corrections and real corrections with one extra parton in the final state. There are two types of real corrections: gluon-quark-radiated processes $q\bar{q}' \to HVV'g$ where the gluon is radiated off an initial (anti)quark, and gluon-quark-induced processes $qg \to HVV'q'$ where the gluon splits into two quarks leading to a quark-antiquark annihilation process. The virtual corrections are regularized with a dimensional regularization scheme both for the ultraviolet (UV) and infrared (IR) divergences. The generic one-loop diagrams contain triangle, self-energy and box diagrams including a virtual gluon as well as tree-level diagrams involving counterterms and are generated with `FeynArts-3.7` [27]. The one-loop amplitudes are calculated with `FormCalc-7.5` [28] and the scalar integrals [29] are implemented with `LoopTools-2.12` [28, 30]. After the on-shell renormalization of the quark wave functions as well as the CKM matrix elements (when needed) has been performed we are still left with soft and collinear IR divergences.

Our calculation is implemented in the framework of the `POWHEG-BOX` [25]. We make use of the build tool based on `MadGraph 4` [31–33], that was first applied in Ref. [34] and is now routinely used and provided with the public distribution of the `POWHEG-BOX`, in order to generate the Born, the color- and spin-correlated Born and the real-emission amplitudes in a format that can easily be processed. The spin- and color-correlated Born amplitudes are needed for the construction of the counterterms for IR singular configurations in the framework of the Frixione-Kunszt-Signer (FKS) subtraction formalism [35] that is implemented in the `POWHEG-BOX`. The subtracted virtual and real contributions are then separately IR finite up to leftover collinear singularities that are absorbed into the quark PDFs. For the parametrization of the phase space, we adapt the implementation of Ref. [36] that was developed for the case of $t\bar{t}H$ production at the LHC in the `POWHEG-BOX`. This offers the possibility to mimic the

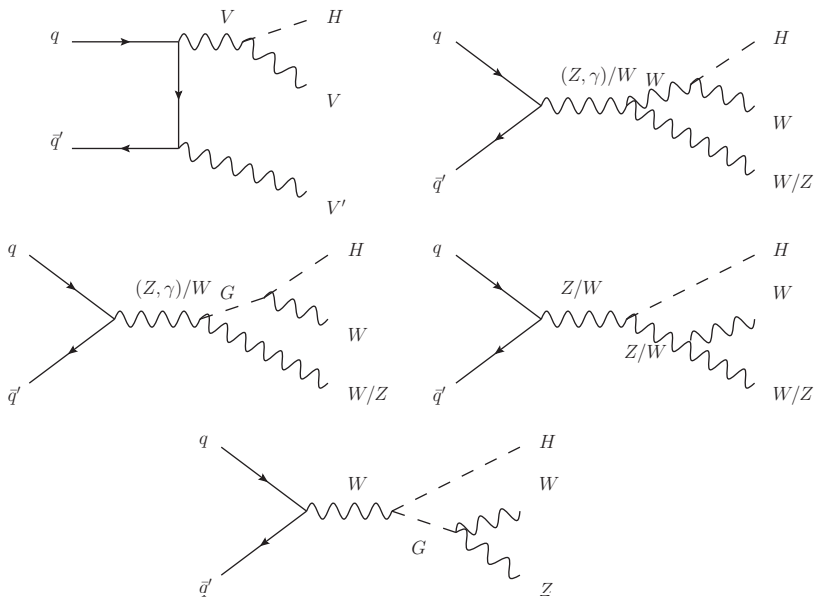

FIG. 1. Representative tree-level diagrams for $q\bar{q}' \to HVV'$ production processes. V, V' stand for W and Z bosons. Only the first generic diagram of the upper row contributes to the HZZ process, while the generic diagram of the lower row only contributes to the $HW^{\pm}Z$ process.

effect of the Higgs width with a smearing of the Higgs four-momentum.

Our calculation has been cross-checked in two ways: by checking that in the collinear limit the contributions from the singular real emission and the subtracting FKS counterterms are equal, and by comparing with the results available in the literature for the $HW^{\pm}Z$ process [21] and for the $HW^{+}W^{-}$ process [20]. Adapting the calculation to the framework of Ref. [21] which only uses the first-generation quarks, a good agreement has been found at NLO with the W charge asymmetry given in their paper. In the case of $pp \to q\bar{q} \to HW^{+}W^{-}$ cross section, the framework of Ref. [20] uses only the $u\bar{u}$ and $d\bar{d}$ partonic subprocesses at NLO, while using all four flavors at Born level. A very good agreement has been found with their results provided that we adapt our calculation to their framework. Note that the authors of Ref. [20] discarded the NLO contributions from $c\bar{c}$ and $s\bar{s}$ partonic subprocesses, arguing that the respective LO contributions are already only a bit less than $\sim 10\%$ of the full LO hadronic cross section, hence the putative NLO contributions would be negligible. However we find that these NLO corrections are of the order of 4% as they follow the same pattern as the dominant $u\bar{u} + d\bar{d}$ contributions, that is a +40% increase over the LO cross section. This is of the same order as the gluon fusion contribution they include in their analysis of the higher order contributions. We feel that if one wants to add higher-order terms that go beyond NLO, e.g. NNLO terms, one should also include all the lower order corrections that have at least the same effects as these new NNLO terms.

III. DIFFERENTIAL CROSS SECTIONS AND PARTON SHOWER EFFECTS

We present in this section the differential distributions, focusing on the Higgs transverse momentum $p_{T,H}$, the weak boson pair invariant mass $M_{VV'}$ and the jet transverse momentum $p_{T,j}$ histograms, where V/V' stands for one of the weak bosons. The setup of the calculation is defined in Sec. III A and will be used for the distributions as well as for the study of the uncertainties affecting the total rates presented in Sec. IV. Parton shower effects, in particular in the $p_{T,j}$ distributions, will be discussed.

A. Setup of The Calculation

We follow the LHC Higgs Cross Section Working Group [37] recommendation and use the following set of input parameters,

$$\begin{aligned} &G_F = 1.16637 \times 10^{-5}\ \text{GeV}^{-2},\ M_W = 80.385\ \text{GeV}, \\ &M_Z = 91.1876\ \text{GeV},\ M_t = 172.5\ \text{GeV}, \\ &M_H = 125\ \text{GeV},\ \alpha_s^{\text{NLO}}(M_Z^2) = 0.118, \end{aligned} \tag{4}$$

where all but M_H is taken from Ref. [38]. The CKM matrix is assumed to be diagonal except in $HW^{\pm}Z$ channels where the numerical values for the CKM matrix elements are taken from Ref. [38]. The masses of the light quarks are approximated as zero. This is justified by the insensitiveness of the results to those masses. The parametric uncertainties on the input parameters will be discussed in Sec. IV when presenting the results on total rates. Following the latest PDF4LHC Recommendation [39] we use

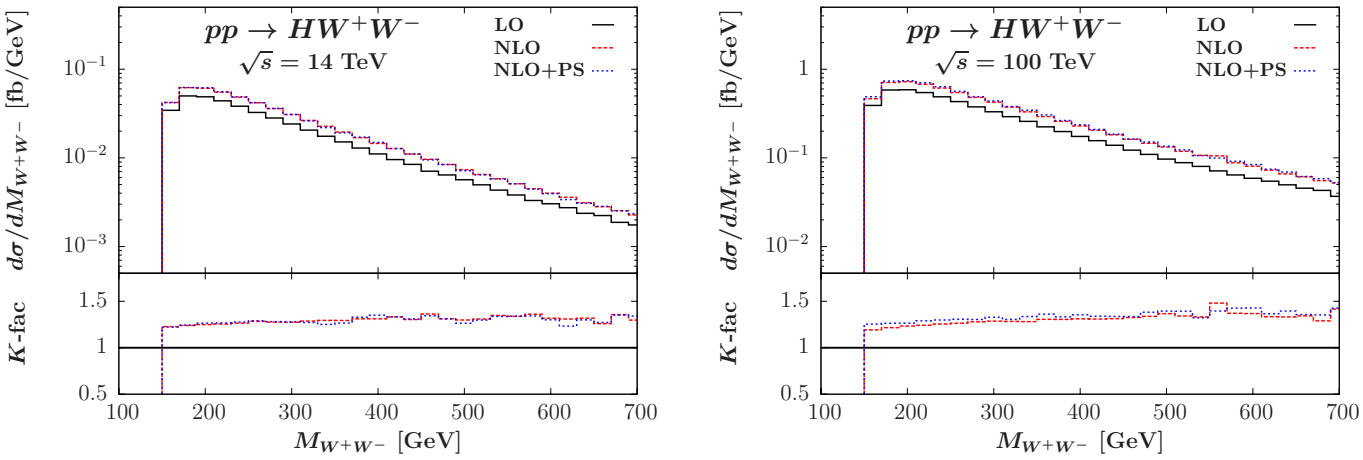

FIG. 2. In the main frame: W pair invariant mass $M_{W^+W^-}$ (in GeV) distribution of the $pp \to HW^+W^-$ cross section (in fb/GeV) at the 14 TeV LHC (left) and at the 100 TeV FCC-hh (right) calculated with the `PDF4LHC15_nlo` PDF set and with the input parameters given in Eq. (4). In blue (thin dotted): LO predictions; in red (dashed): NLO predictions; in green (dotted): NLO predictions including PS effects. In the insert are displayed the NLO and NLO+PS K–factors relative to the LO prediction.

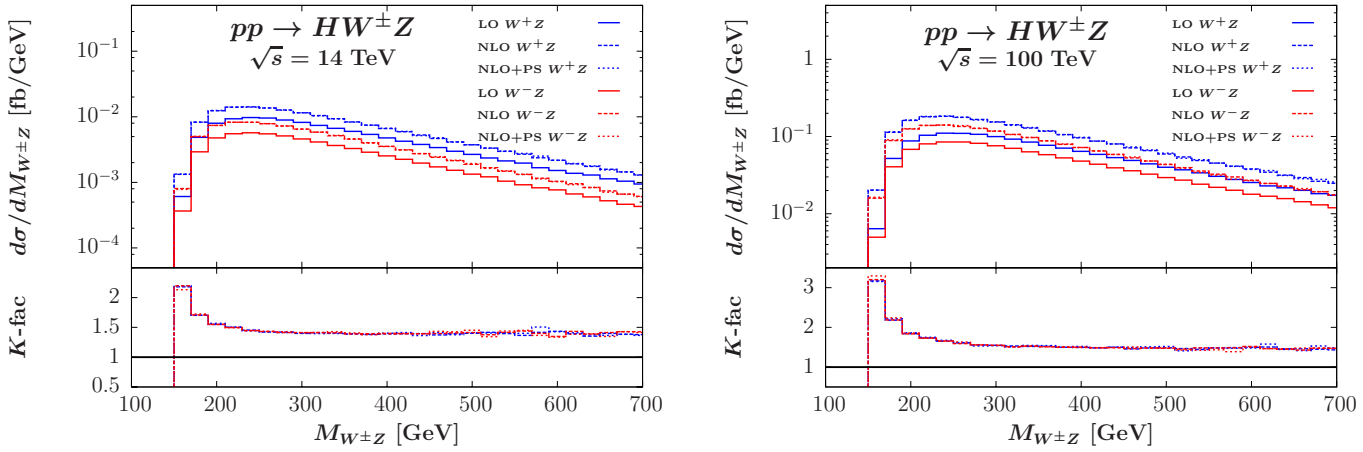

FIG. 3. In the main frame: $W^\pm Z$ pair invariant mass $M_{W^\pm Z}$ (in GeV) distribution of the $pp \to HW^\pm Z$ cross section (in fb/GeV) at the 14 TeV LHC (left) and at the 100 TeV FCC-hh (right) calculated with the `PDF4LHC15_nlo` PDF set and with the input parameters given in Eq. (4). The predictions for the W^+Z channel are in blue, the predictions for the W^-Z channel are in red. With thin dotted lines: LO predictions; with dashed lines: NLO predictions; with dotted line: NLO predictions including PS effects. In the insert are displayed the NLO and NLO+PS K–factors relative to the LO predictions.

in the `LHAPDF6` framework [40] the NLO PDF set family `PDF4LHC15_nlo` which combines in a consistent statistical framework the three global sets `CT14` [41], `MMHT14` [42] and `NNPDF3.0` [43]. We use `FastJet` for the parton shower [44, 45]. The central scale choice is defined as the invariant Higgs+2 weak boson mass. More specifically we will use $\mu_R = \mu_F = \mu_0$ with

$$\mu_0^{HWW} = M_{HW^+W^-},\ \mu_0^{HWZ} = M_{HW^\pm Z},$$
$$\mu_0^{HZZ} = M_{HZZ}. \qquad (5)$$

In order to quantify the importance of the NLO QCD corrections we have first calculated the total cross sections at the central scales given above before studying the differential distributions. We have found that they are significant in all channels. They lead to an increase of the $HW^\pm Z$ cross sections by $\sim +43\%$ at LHC energies and $\sim +55\%$ at the FCC-hh at 100 TeV, similar to what has been observed earlier in the literature in the case of the LHC, albeit with a different central scale choice of $\mu_0 = \frac{1}{2}(M_W + M_Z + M_H)$ [21]. The increase is more moderate in the case of the HW^+W^- cross section with a $\sim +27\%$ over the whole c.m. energy range and even more reduced in the case of the HZZ cross section where the increase is $\sim +23\%$ at 13 TeV and down to $\sim +17\%$ at 100 TeV.

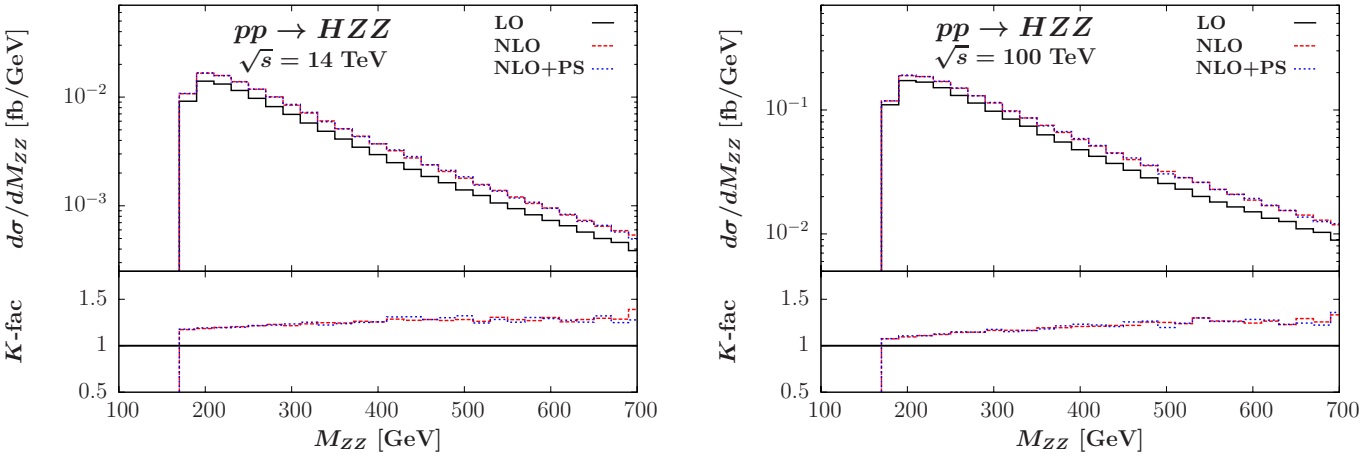

FIG. 4. In the main frame: Z pair invariant mass M_{ZZ} (in GeV) distribution of the $pp \to HZZ$ cross section (in fb/GeV) at the 14 TeV LHC (left) and at the 100 TeV FCC-hh (right) calculated with the `PDF4LHC15_nlo` PDF set and with the input parameters given in Eq. (4). In blue (thin dotted): LO predictions; in red (dashed): NLO predictions; in green (dotted): NLO predictions including PS effects. In the insert are displayed the NLO and NLO+PS K–factors relative to the LO prediction.

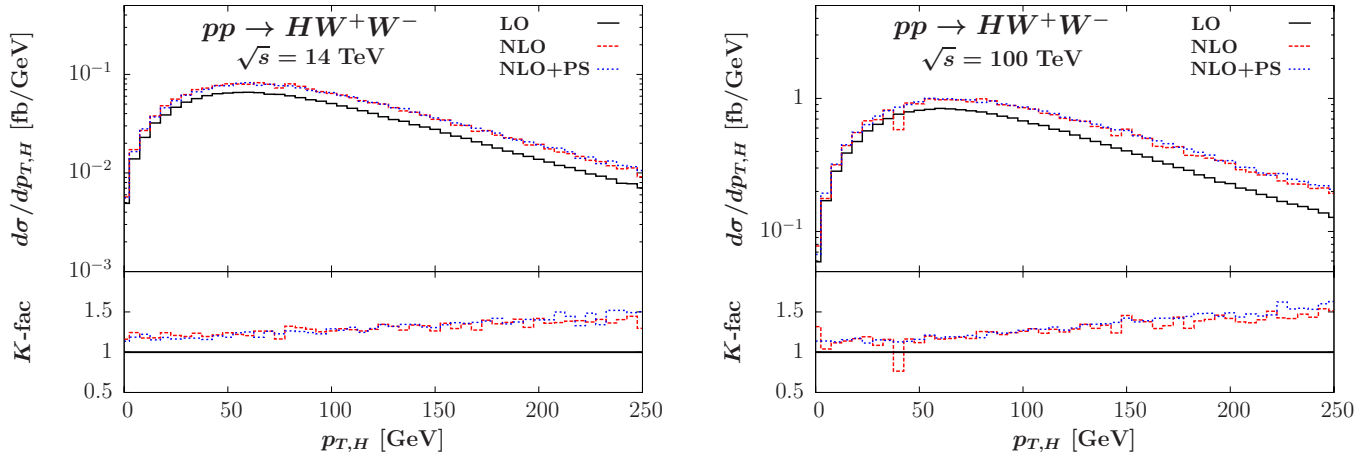

FIG. 5. In the main frame: Higgs transverse momentum $p_{T,H}$ (in GeV) distribution of the $pp \to HW^+W^-$ cross section (in fb/GeV) at the 14 TeV LHC (left) and at the 100 TeV FCC-hh (right) calculated with the `PDF4LHC15_nlo` PDF set and with the input parameters given in Eq. (4). In blue (thin dotted): LO predictions; in red (dashed): NLO predictions; in green (dotted): NLO predictions including PS effects. In the insert are displayed the NLO and NLO+PS K–factors relative to the LO prediction.

B. VV' Invariant Mass and Higgs Transverse Momentum Distributions

We start the analysis by looking at the distributions of the invariant mass of the weak boson pairs $M_{VV'}$ where $VV' = W^+W^-, W^\pm Z, ZZ$. We study the case of the 14 TeV LHC and the case of the 100 TeV FCC-hh collider. The $M_{W^+W^-}$ distribution in the HW^+W^- channel is displayed in Fig. 2, the $M_{W^\pm Z}$ distributions in the $HW^\pm W^-$ channel are displayed in Fig. 3 and the M_{ZZ} distribution in the HZZ channel is displayed in Fig. 4. We display the LO distributions in blue (thin dotted), the NLO fixed-order distributions in red (dashed) and the NLO+PS results in green (dotted). The inserts show the K–factors with respect to the LO predictions, the latter being calculated with an NLO PDF set (no LO PDF set exists in the `PDF4LHC15` family) but using a LO evolution for the splitting functions with a LO α_S evolution. The two Z bosons in $pp \to HZZ$ are p_T ordered.

The shapes are the same at 14 TeV and 100 TeV in all channels. The NLO effects are nearly overall rescaling factors as the K–factors only rise very mildly and linearly, from $K \sim 1.2$ to $K \sim 1.3$ at 14 TeV (to $K \sim 1.4$ at 100 TeV) in the case of the $M_{W^+W^-}$ and M_{ZZ} distributions. The distributions for the $HW^\pm Z$ channels display a slightly different behavior, the K–factors being flat for $M_{W^\pm Z} \geq 200$ GeV with $K \sim 1.5$, after a peak at the $W^\pm Z$ threshold. We should also stress that these distributions show no additional effects from the shower on top of the NLO QCD corrections.

We also display the Higgs transverse momentum distributions, in Fig. 5 for the HW^+W^- channel, in Fig. 6

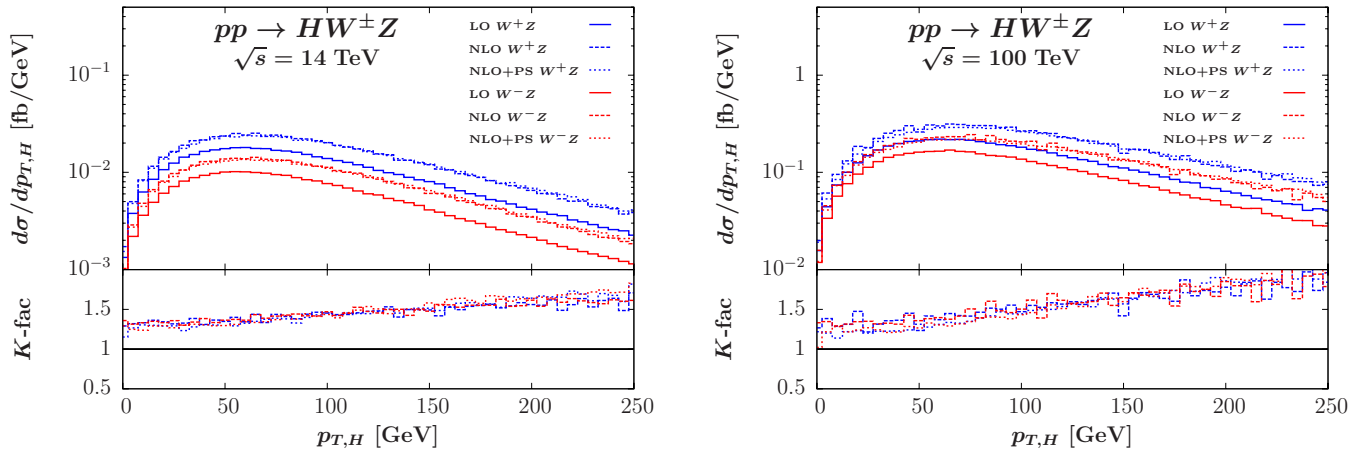

FIG. 6. In the main frame: Higgs transverse momentum $p_{T,H}$ (in GeV) distribution of $pp \to HW^{\pm}Z$ cross section (in fb/GeV) at the 14 TeV LHC (left) and at the 100 TeV FCC-hh (right) calculated with `PDF4LHC15_nlo` PDF set and with the input parameters given in Eq. (4). The predictions for the W^+Z channel are in blue, the predictions for the W^-Z channel are in red. With thin dotted lines: LO predictions; with dashed lines: NLO predictions; with dotted line: NLO predictions including PS effects. In the insert are displayed the NLO and NLO+PS K–factors relative to the LO predictions.

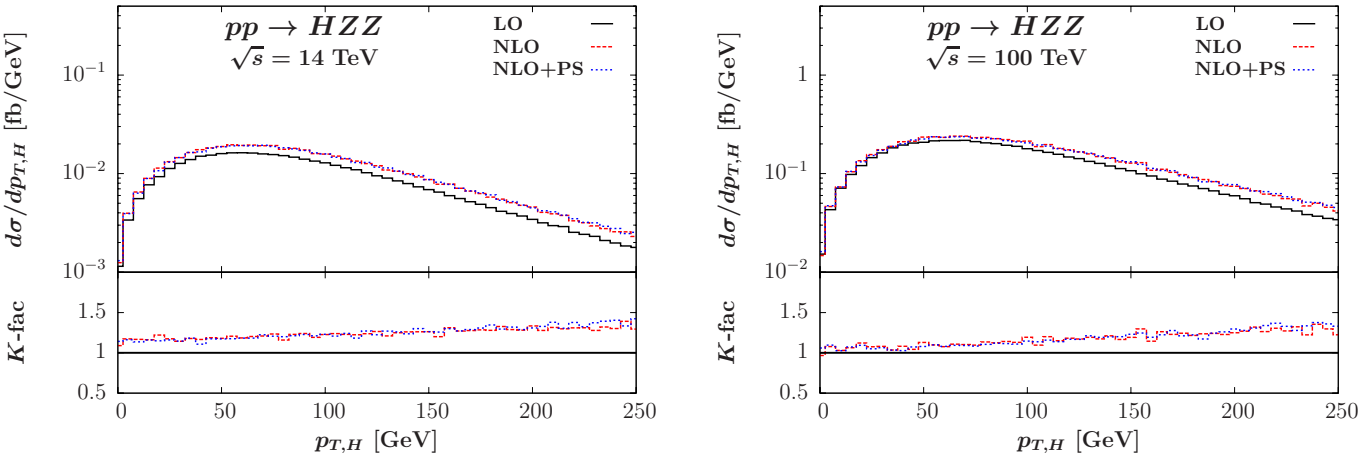

FIG. 7. In the main frame: Higgs transverse momentum $p_{T,H}$ (in GeV) distribution of $pp \to HZZ$ cross section (in fb/GeV) at the 14 TeV LHC (left) and at the 100 TeV FCC-hh (right) calculated with `PDF4LHC15_nlo` PDF set and with the input parameters given in Eq. (4). In blue (thin dotted): LO predictions; in red (dashed): NLO predictions; in green (dotted): NLO predictions including PS effects. In the insert are displayed the NLO and NLO+PS K–factors relative to the LO prediction.

for the $HW^{\pm}Z$ channels and in Fig. 7 for the HZZ channel. The color code and the inserts follow the same conventions described in the case of the invariant mass distributions. Going from 14 TeV to 100 TeV changes nearly nothing in the HW^+W^- and HZZ channels as far as the K–factors are concerned and the PS effects are again negligible. The K–factor reaches 1.5 at 100 TeV at $p_{T,H} = 250$ GeV in the HW^+W^- channel. The increase in the K–factor is even smaller in the HZZ channel with $K \sim 1.3$ at 100 TeV. In contrast, the $HW \pm Z$ channels display a strong dependence on the K–factors with respect to the Higgs transverse momentum. The increase is again linear but steeper, especially at 100 TeV where $K \sim 1.3$ at low p_T to reach more than 2 at $p_{T,H} = 250$ GeV. Again the PS effects are negligible and the two channels HW^+Z and HW^-Z display an identical behavior.

C. Jet Transverse Momentum Distributions

In order to investigate the impact of the PS effects we display the jet transverse momentum distribution in Fig. 8 for the HW^+W^- channel, in Fig. 9 for the $HW^{\pm}Z$ channels and in Fig. 10 for the HZZ channel. We display the NLO and the NLO+PS distributions and the insert shows the ratio between the two predictions, to clearly emphasize the PS effects. It is clear that the fixed-order results do not properly account for the behavior at low p_T, and this is where the PS effects are sizable. The NLO+PS distributions display the correct behavior thanks to the resummation of soft gluon effects.

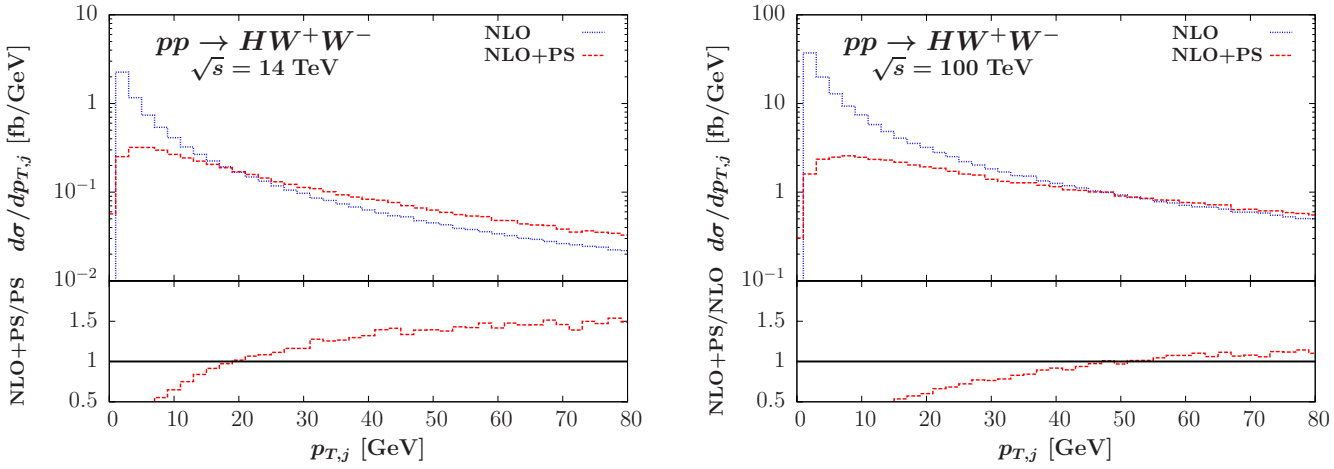

FIG. 8. In the main frame: Jet transverse momentum $p_{T,j}$ (in GeV) distribution of the $pp \to HW^+W^-$ cross section (in fb/GeV) at the 14 TeV LHC (left) and at the 100 TeV FCC-hh (right) calculated with the `PDF4LHC15_nlo` PDF set and with the input parameters given in Eq. (4). In blue (thin dotted): the NLO prediction; in red (dashed): the NLO predictions including PS effects. In the insert is displayed the ratio between the NLO+PS and the NLO predictions.

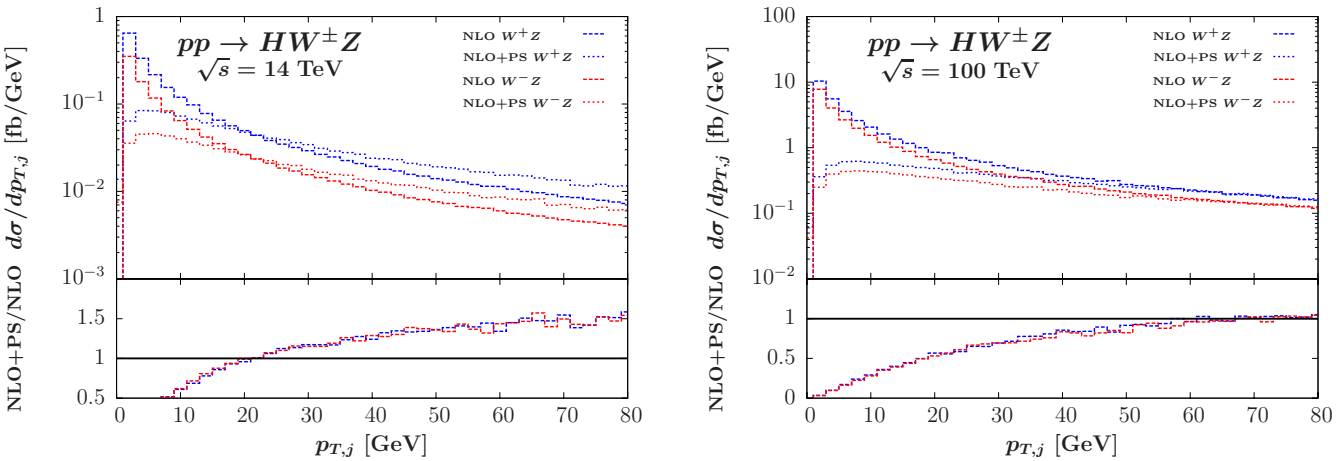

FIG. 9. In the main frame: Jet transverse momentum $p_{T,j}$ (in GeV) distribution of the $pp \to HW^\pm Z$ cross section (in fb/GeV) at the 14 TeV LHC (left) and at the 100 TeV FCC-hh (right) calculated with the `PDF4LHC15_nlo` PDF set and with the input parameters given in Eq. (4). The predictions for the W^+Z channel are in blue, the predictions for the W^-Z channel are in red. With dashed lines: NLO predictions; with dotted line: NLO predictions including PS effects. In the insert is displayed the ratio between the NLO+PS and the NLO predictions.

Going from 14 TeV to 100 TeV leads to K–factors reaching 1 at high p_T while these are slightly larger at 14 TeV. This means the fixed-order NLO results are much closer to the NLO+PS results at 100 TeV than at 14 TeV for high values of the jet transverse momentum.

IV. TOTAL CROSS SECTIONS AT THE LHC AND AT THE FCC-HH INCLUDING THEORETICAL UNCERTAINTIES

The total rates are affected by several uncertainties that we will study in this last section. We will consider three sources of uncertainties: the scale uncertainty which can be roughly viewed as an estimate of the missing higher-order terms in the perturbative calculation, the uncertainty related to the parton distribution functions and the fitted value of the strong coupling constant $\alpha_s(M_Z^2)$ and the parametric uncertainties related to the experimental errors on W and Z masses, $M_W = (80.385 \pm 0.015)$ GeV and $M_Z = (91.1876 \pm 0.0021)$ GeV as given by Ref. [38].

As far as the parametric uncertainties on the input masses are concerned, it has been checked that they do not exceed more than $\pm 0.1\%$ at all c.m. energies in all channels. These errors will then be ignored in the following and in particular in the final combination of all the uncertainties.

We use the same parameter setup as in Section III and our chosen PDF set is `PDF4LHC15_nlo_30_pdfas`

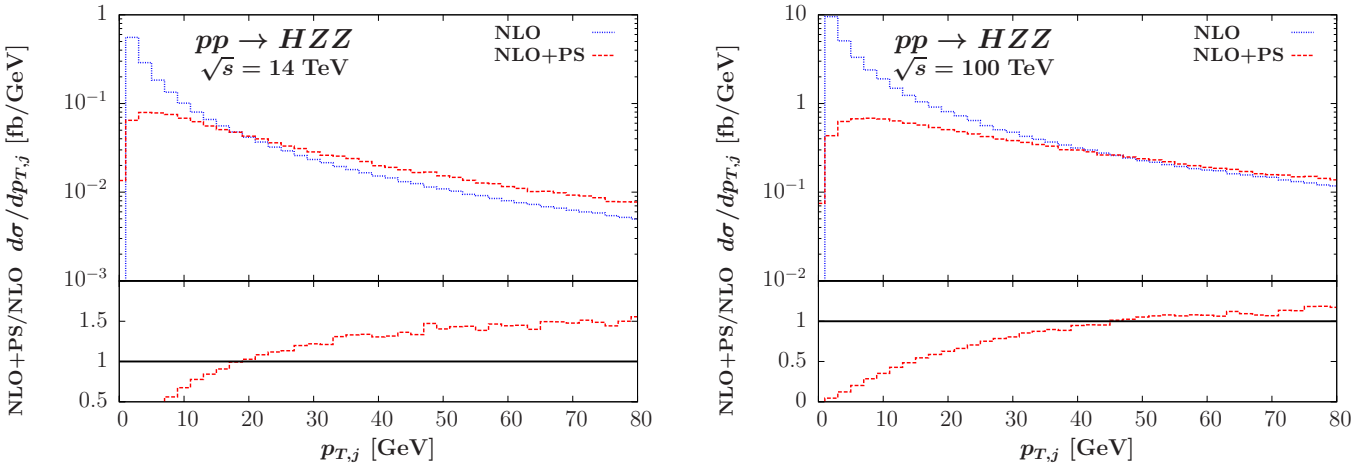

FIG. 10. In the main frame: Jet transverse momentum $p_{T,j}$ (in GeV) distribution of $pp \to HZZ$ cross section (in fb/GeV) at the 14 TeV LHC (left) and at the 100 TeV FCC-hh (right) calculated with the `PDF4LHC15_nlo` PDF set and with the input parameters given in Eq. (4). In blue (thin dotted): the NLO prediction; in red (dashed): the NLO prediction including PS effects. In the insert is displayed the ratio between the NLO+PS and the NLO predictions.

that uses for the strong coupling constant $\alpha_s(M_Z^2) = 0.1180 \pm 0.0015$. We recall that the running of α_s is evaluated at NLO.

A. Scale Uncertainty

As the calculation is done in the perturbative framework, the theoretical cross sections depend on two unphysical scales: the renormalization scale μ_R that comes from the running of α_s, and the factorization scale μ_F that comes from the convolution of the perturbative partonic cross sections with the nonperturbative parton distribution functions. The variation of the cross sections with respect to these two scales gives the confidence of the prediction calculated with a given central scale. This is often viewed as an estimate of the missing higher-order corrections even if this interpretation should be taken with care[46]. We choose the interval

$$\frac{1}{2}\mu_0 \leq \mu_R = \mu_F \leq 2\,\mu_0\,, \tag{6}$$

where μ_0 is the central scale for the process under study and has been defined in Eq. (5).

As can be seen in Fig. 11, the scale uncertainty is small in the different gauge boson pair production channels: we obtain $\sim +2\%/-1.5\%$ at 13 TeV in HW^+W^- and HZZ channels, a bit more in $HW^\pm Z$ channels with $\sim +3.5\%/-3\%$ at 13 TeV. It then increases at 100 TeV to reach $\sim +4\%/-5\%$ in HW^+W^- channel and $\sim +5\%/-6\%$ in $HW^\pm Z$ channels, slightly less in HZZ channel with $\sim +3\%/-4\%$.

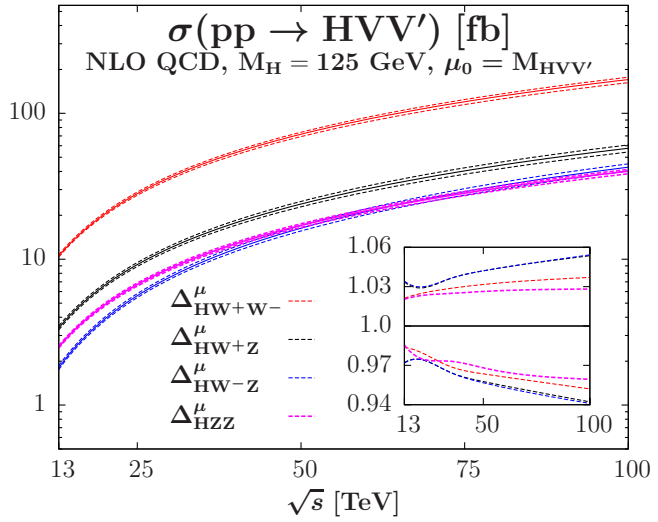

FIG. 11. Scale uncertainty for a scale variation in the interval $\frac{1}{2}\mu_0 \leq \mu_R = \mu_F \leq 2\mu_0$ in $\sigma(pp \to HW^+W^-, W^\pm Z, ZZ)$ (in fb) at the LHC and FCC-hh as a function of the c.m. energy (in TeV). In the inserts the relative deviations from the central cross section obtained with $\mu_R = \mu_F = \mu_0 = M_{HVV'}$ are shown.

B. PDF+α_s Uncertainty

The other source of theoretical uncertainty that is considered in this calculation stems from the parametrization of the parton distribution functions (PDF). The calculation of an hadronic cross section can be separated into two parts: the hard cross section is calculated at the parton level in a perturbative framework, and the result is then convoluted at the factorization scale μ_F with the nonperturbative PDFs that describe the probability of extracting from the proton a given parton with a mo-

mentum fraction x of the initial proton. The PDFs are the result of a fit on experimental data sets, leading to an uncertainty on the calculated cross section.

There exist numerous sets on the market, some of which including now jet data from the LHC Run 1. There have been many improvements in the last years towards a more unified approach resulting in the 2015 PDF4LHC Recommendation [39]. The current prescription is to use one of the combined sets resulting from a consistent statistical treatment of the three global sets `CT14` [41], `MMHT14` [42] and `NNPDF3.0` [43], following the work of Ref. [47]. We use the Hessian version of this combined set at NLO with 30 error sets, `PDF4LHC15_nlo_30`, in order to calculate the uncertainties due to the PDFs [48, 49]. We start by calculating the central prediction σ^0 with the central PDF set, and then the 30 different cross sections σ^k using the 30 error sets of `PDF4LHC15_nlo_30`, $k = 1...30$. The 68%CL PDF uncertainty is calculated using the following formula [39],

$$\Delta^{\rm PDF}\sigma = \sqrt{\sum_{k=1}^{30}(\sigma^k - \sigma^0)^2}. \qquad (7)$$

The PDF uncertainty is thus symmetric.

In addition to this PDF uncertainty there exists an uncertainty related to the determination of the strong coupling constant α_s. In the `PDF4LHC15` sets the current value of the strong coupling constant and of its associated uncertainty are that of the Particle Data Group [38],

$$\alpha_s(M_Z^2) = 0.1180 \pm 0.0015, \qquad (8)$$

at the 68%CL and at NLO. To calculate the combined PDF+α_s uncertainty we first use the sets 31 and 32 of `PDF4LHC15_nlo_30_pdfas` to obtain $\sigma^-_{\alpha_s}$ and $\sigma^+_{\alpha_s}$ corresponding to $\alpha_s(M_Z^2) = 0.1165$ and $\alpha_s(M_Z^2) = 0.1195$. We then calculate the 68%CL α_s–uncertainty using [39]

$$\Delta^{\alpha_s}\sigma = \frac{1}{2}\left|\sigma^+_{\alpha_s} - \sigma^-_{\alpha_s}\right|, \qquad (9)$$

that is eventually combined in quadrature with $\Delta^{\rm PDF}\sigma$ to obtain the final 68%CL PDF+α_s uncertainty,

$$\Delta^{\rm PDF+\alpha_s}\sigma = \sqrt{(\Delta^{\rm PDF}\sigma)^2 + (\Delta^{\alpha_s}\sigma)^2}. \qquad (10)$$

The results for the PDF and PDF+α_s uncertainties are displayed in Fig. 12. The PDF uncertainties are of order $\pm 2\%$ in all channels at the 13/14 TeV LHC. In the case of HW^+W^- production this uncertainty is also nearly the same at the FCC-hh at 100 TeV, while it reduces to $\pm 1.5\%$ in the $HW^\pm Z$ channels and stays at the same level in the HZZ channel. The effect of the additional α_s uncertainty is negligible at low energies and increases the PDF uncertainty by $\sim 0.5\%$ at higher energies in all channels.

C. Total Uncertainty in the Three Channels

We can now present the final results including the total theoretical uncertainty in the different channels. We add linearly the scale and PDF+α_s uncertainty following the LHC Higgs Cross Section Working Group [50] and do not include the parametric uncertainties due to the experimental errors on the input weak boson masses as they are found to be negligible. The end result is displayed in Fig. 13 and detailed in Tables I, II and III which also includes the individuals numbers for the scale, PDF and PDF+α_s uncertainties. The total uncertainties are small in the whole c.m. energy range, being $\sim \pm 4\%$ at 13/14 TeV for the HW^+W^- and HZZ channels, and slightly more for the $HW^\pm Z$ channel with $\sim +6\%/-5\%$. At the FCC-hh at 100 TeV the total uncertainties increase slightly to $\pm 6\%/8\%$ for the various channels.

V. CONCLUSIONS

We have presented in this paper the NLO QCD analysis of the production of a SM Higgs boson in association with a pair of massive weak bosons, at a proton-proton collider starting from LHC energies of 13/14 TeV up to the FCC-hh energy of 100 TeV. We have calculated the QCD corrections in the `POWHEG-BOX` framework, including an interface to parton shower. This is the first calculation of the NLO QCD corrections for the HZZ channel and this is the first presentation of parton-shower effects for the three processes HW^+W^-, $HW^\pm Z$ and HZZ. We have found that the QCD corrections are significant and lead to an increase of the $HW^\pm Z$ cross sections by $\sim +43\%$ at LHC energies and $\sim +55\%$ at the FCC-hh at 100 TeV when using the invariant mass of the three massive final-state particles as a central scale, similar to what has been observed earlier in the literature. The increase is more moderate in the case of the HW^+W^- cross section with a $\sim +27\%$ over the whole c.m. energy range and even more reduced in the case of the HZZ cross section where the increase is $\sim +23\%$ at 13 TeV and down to $\sim +17\%$ at 100 TeV. In order to have meaningful results these QCD corrections have to be included in any phenomenological analysis. In Section III we have studied the differential distributions, focusing in particular on the $M_{VV'}$, the $p_{T,H}$ and the $p_{T,j}$ distributions where V, V' stand for the various weak bosons considered. The K–factors are nearly flat in many of the distributions with only a very mild linear increase, with the notable exception of the Higgs p_T distribution in the $HW^\pm Z$ channel where it rises from ~ 1.3 up to ~ 2 at $p_{T,H} = 250$ GeV. The shapes are not different when going from 14 TeV to 100 TeV. The parton shower effects are very small except in the case of the jet p_T distribution where they correct the bad behavior of the fixed-order calculation at low p_T, as expected. In Section IV we have presented the numerical results for the total cross sections including the theoretical uncertainties affecting the predictions. It has

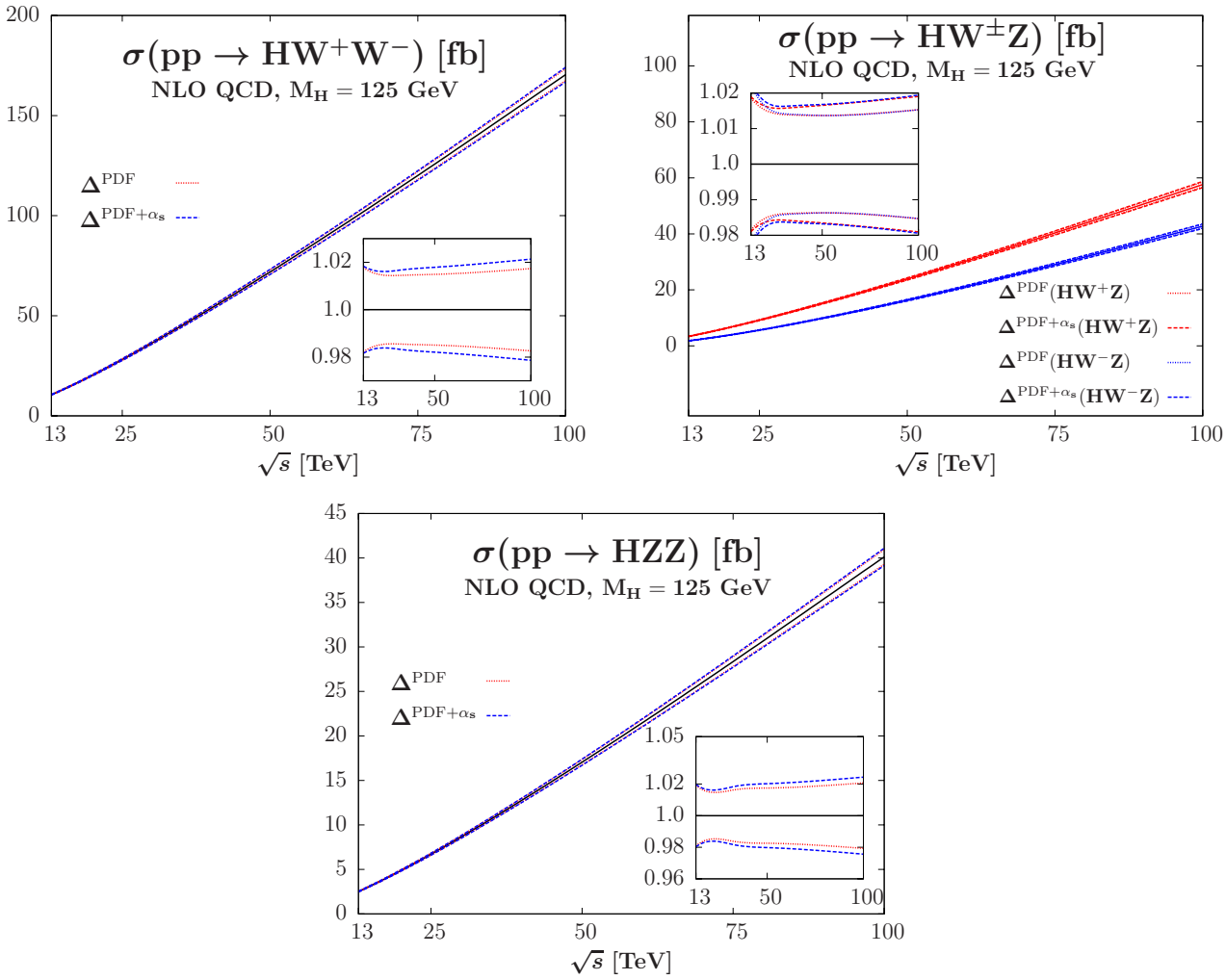

FIG. 12. PDF and PDF+α_s uncertainties using the `PDF4LHC15_nlo_30_pdfas` PDF set in $\sigma(pp \to HW^+W^-, HW^\pm Z, HZZ)$ at the LHC and the FCC-hh (in fb) as a function of the c.m. energy (in TeV). Upper left: HW^+W^- cross section. Upper right: $HW^\pm Z$ cross sections. Lower: HZZ cross section. The relative deviations from the central cross sections are shown in the inserts of the three individual figures.

TABLE I. The total HW^+W^- production cross section at NLO QCD at the LHC and the FCC-hh (in fb) for given c.m. energies (in TeV) at the central scale $\mu_F = \mu_R = M_{HW^+W^-}$. The corresponding shifts due to the theoretical uncertainties coming from scale variation, PDF, PDF+α_s errors, as well as the total uncertainty when all errors are added linearly, are shown.

$\sqrt{s}$ [TeV]	$\sigma^{\rm NLO}_{HWW}$ [fb]	Scale [%]	PDF [%]	PDF +α_s [%]	Total [%]
13	10.5	$^{+2.1}_{-1.6}$	$^{+1.8}_{-1.8}$	$^{+1.8}_{-1.8}$	$^{+4.0}_{-3.5}$
14	11.8	$^{+2.2}_{-1.7}$	$^{+1.7}_{-1.7}$	$^{+1.8}_{-1.8}$	$^{+4.0}_{-3.5}$
33	41.5	$^{+2.8}_{-3.0}$	$^{+1.5}_{-1.5}$	$^{+1.7}_{-1.7}$	$^{+4.5}_{-4.7}$
100	170	$^{+3.7}_{-4.8}$	$^{+1.7}_{-1.7}$	$^{+2.1}_{-2.1}$	$^{+5.8}_{-6.9}$

been found that the global hierarchy between the three channels, HW^+W^-, HW^+Z+HW^-Z and HZZ is similar to that of weak boson pair production, albeit with a small change when considering the HW^+Z and HW^-Z channels separately; in the latter case HZZ dominates over HW^-Z at lower c.m. energies while the ZZ cross section is always smaller than the W^-Z cross section. The ratio is 4:2:1 for $HWW : HWZ : HZZ$. The parametric errors on the input W and Z boson masses are found to be negligible in all channels at all c.m. energies.

TABLE II. Same as Table I but for the HW^+Z and HW^-Z channels at the central scale $\mu_F = \mu_R = M_{HW^\pm Z}$.

$\sqrt{s}$ [TeV]	$\sigma^{\rm NLO}_{HW^+Z}$ [fb]	Scale [%]	PDF [%]	PDF $+\alpha_s$ [%]	Total [%]
13	3.37	$+3.4$ -2.8	$+1.9$ -1.9	$+1.9$ -1.9	$+5.3$ -4.7
14	3.81	$+3.2$ -2.7	$+1.8$ -1.8	$+1.8$ -1.8	$+5.1$ -4.5
33	13.6	$+3.5$ -3.4	$+1.4$ -1.4	$+1.6$ -1.6	$+5.1$ -5.0
100	57.6	$+5.4$ -5.8	$+1.5$ -1.5	$+1.9$ -1.9	$+7.3$ -7.7

$\sqrt{s}$ [TeV]	$\sigma^{\rm NLO}_{HW^-Z}$ [fb]	Scale [%]	PDF [%]	PDF $+\alpha_s$ [%]	Total [%]
13	1.80	$+3.4$ -2.8	$+2.2$ -2.2	$+2.3$ -2.3	$+5.7$ -5.1
14	2.07	$+3.3$ -2.7	$+2.1$ -2.1	$+2.2$ -2.2	$+5.5$ -4.9
33	8.76	$+3.5$ -3.4	$+1.4$ -1.4	$+1.6$ -1.6	$+5.2$ -5.1
100	42.7	$+5.4$ -5.9	$+1.5$ -1.5	$+1.9$ -1.9	$+7.4$ -7.8

TABLE III. Same as Table I but for the HZZ channel at the central scale $\mu_F = \mu_R = M_{HZZ}$.

$\sqrt{s}$ [TeV]	$\sigma^{\rm NLO}_{HZZ}$ [fb]	Scale [%]	PDF [%]	PDF $+\alpha_s$ [%]	Total [%]
13	2.50	$+2.0$ -1.4	$+1.9$ -1.9	$+2.0$ -2.0	$+4.0$ -3.4
14	2.82	$+2.1$ -1.6	$+1.8$ -1.8	$+1.9$ -1.9	$+4.0$ -3.5
33	9.86	$+2.5$ -2.7	$+1.6$ -1.6	$+1.8$ -1.8	$+4.3$ -4.5
100	40.1	$+2.8$ -4.1	$+2.1$ -2.1	$+2.4$ -2.4	$+5.2$ -6.5

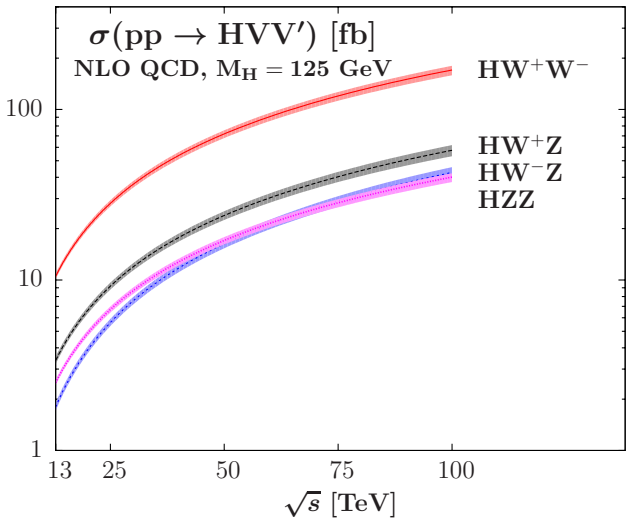

FIG. 13. The total cross sections (in fb) for SM Higgs production in association with a pair of weak bosons at NLO QCD as a function of the c.m. energy (in TeV) with $M_H = 125$ GeV: HW^+W^- (red/full), HW^+Z (gray/dashed), HW^-Z (pink/dotted) and HZZ (blue/dashed with small dashes). The `PDF4LHC2015_30` PDF set has been used and the theoretical uncertainties are included as corresponding bands around the central values.

Using the 2015 PDF4LHC Recommendation we have calculated the PDF+α_s uncertainty that has been combined with the scale uncertainty and the final theoretical uncertainty is found to be small, no more than $\sim \pm 7\%$ at 100 TeV and less that $\sim \pm 5\%$ at 13/14 TeV. A public release of the code in the `POWHEG-BOX` is expected in the near future so that the community can use the three presented processes in the study of the Higgs gauge couplings.

ACKNOWLEDGMENTS

The author thanks Barbara Jäger, Lukas Salfelder, Matthias Kesenheimer and Ning Liu for useful discussions. He was supported in part by the Institutional Strategy of the University of Tübingen (DFG, ZUK 63) and the DFG Grant JA 1954/1. This work was performed on the computational resource bwUniCluster funded by the Ministry of Science, Research and the Arts Baden-Württemberg and the Universities of the State of Baden-Württemberg, Germany, within the framework program bwHPC.

[1] G. Aad *et al.* (ATLAS Collaboration), Phys.Lett., **B716**, 1 (2012), arXiv:1207.7214 [hep-ex].

[2] S. Chatrchyan *et al.* (CMS Collaboration), Phys.Lett., **B716**, 30 (2012), arXiv:1207.7235 [hep-ex].

[3] P. W. Higgs, Phys.Lett., **12**, 132 (1964).
[4] F. Englert and R. Brout, Phys.Rev.Lett., **13**, 321 (1964).
[5] P. W. Higgs, Phys.Rev.Lett., **13**, 508 (1964).
[6] G. Guralnik, C. Hagen, and T. Kibble, Phys.Rev.Lett., **13**, 585 (1964).
[7] G. Aad *et al.* (ATLAS), Phys.Rev., **D91**, 012006 (2015), arXiv:1408.5191 [hep-ex].
[8] V. Khachatryan *et al.* (CMS), Phys. Rev., **D92**, 012004 (2015), arXiv:1411.3441 [hep-ex].
[9] G. Aad *et al.* (ATLAS Collaboration), *Study of the spin and parity of the Higgs boson in HVV decays with the ATLAS detector*, Tech. Rep. ATLAS-CONF-2015-008 (CERN, 2015).
[10] G. Belanger, B. Dumont, U. Ellwanger, J. Gunion, and S. Kraml, Phys.Rev., **D88**, 075008 (2013), arXiv:1306.2941 [hep-ph].
[11] T. Corbett, O. J. P. Eboli, D. Goncalves, J. Gonzalez-Fraile, T. Plehn, and M. Rauch, JHEP, **08**, 156 (2015), arXiv:1505.05516 [hep-ph].
[12] M. Baillargeon, F. Boudjema, F. Cuypers, E. Gabrielli, and B. Mele, Nucl.Phys., **B424**, 343 (1994), arXiv:hep-ph/9307225 [hep-ph].
[13] K.-m. Cheung, Phys.Rev., **D49**, 6224 (1994).
[14] A. Djouadi, Phys.Rept., **457**, 1 (2008), arXiv:hep-ph/0503172 [hep-ph].
[15] J. Baglio, A. Djouadi, and J. Quevillon, (2015), arXiv:1511.07853 [hep-ph].
[16] E. Gabrielli, M. Heikinheimo, L. Marzola, B. Mele, C. Spethmann, *et al.*, Phys.Rev., **D89**, 053012 (2014), arXiv:1312.4956 [hep-ph].
[17] T. Corbett, O. Éboli, J. Gonzalez-Fraile, and M. Gonzalez-Garcia, Phys.Rev.Lett., **111**, 011801 (2013), arXiv:1304.1151 [hep-ph].
[18] Workshop on FCC-hh, the sub-group Exploration of Electroweak Symmetry Breaking (incl. Higgs), Roberto Contino and Heather Gray (conveners); `https://twiki.cern.ch/twiki/bin/view/LHCPhysics/HiggsEWSymmetry`.
[19] V. Khachatryan *et al.* (CMS Collaboration), *Higgs pair production at the High Luminosity LHC*, Tech. Rep. CMS-PAS-FTR-15-002 (CERN, 2015).
[20] S. Mao, M. Wen-Gan, Z. Ren-You, G. Lei, W. Shao-Ming, *et al.*, Phys.Rev., **D79**, 054016 (2009), arXiv:0903.2885 [hep-ph].
[21] N. Liu, J. Ren, and B. Yang, Phys.Lett., **B731**, 70 (2014), arXiv:1310.6192 [hep-ph].
[22] S. Mao, W. Neng, L. Gang, M. Wen-Gan, Z. Ren-You, *et al.*, Phys. Rev., **D88**, 076002 (2013), arXiv:1310.0946 [hep-ph].
[23] X. Shou-Jian, M. Wen-Gan, G. Lei, Z. Ren-You, C. Chong, *et al.*, J.Phys., **G42**, 065006 (2015), arXiv:1505.03226 [hep-ph].
[24] S. Frixione, P. Nason, and C. Oleari, JHEP, **0711**, 070 (2007), arXiv:0709.2092 [hep-ph].
[25] S. Alioli, P. Nason, C. Oleari, and E. Re, JHEP, **1006**, 043 (2010), arXiv:1002.2581 [hep-ph].
[26] J. Baglio, L. D. Ninh, and M. M. Weber, Phys.Rev., **D88**, 113005 (2013), arXiv:1307.4331.
[27] T. Hahn, Comput.Phys.Commun., **140**, 418 (2001), arXiv:hep-ph/0012260 [hep-ph].
[28] T. Hahn and M. Perez-Victoria, Comput.Phys.Commun., **118**, 153 (1999), arXiv:hep-ph/9807565 [hep-ph].
[29] G. 't Hooft and M. Veltman, Nucl.Phys., **B153**, 365 (1979).
[30] G. van Oldenborgh, Comput.Phys.Commun., **66**, 1 (1991).
[31] H. Murayama, I. Watanabe, and K. Hagiwara, KEK-91-11 (1992).
[32] T. Stelzer and W. Long, Comput.Phys.Commun., **81**, 357 (1994), arXiv:hep-ph/9401258 [hep-ph].
[33] J. Alwall, P. Demin, S. de Visscher, R. Frederix, M. Herquet, *et al.*, JHEP, **0709**, 028 (2007), arXiv:0706.2334 [hep-ph].
[34] J. M. Campbell, R. K. Ellis, R. Frederix, P. Nason, C. Oleari, *et al.*, JHEP, **1207**, 092 (2012), arXiv:1202.5475 [hep-ph].
[35] S. Frixione, Z. Kunszt, and A. Signer, Nucl.Phys., **B467**, 399 (1996), arXiv:hep-ph/9512328 [hep-ph].
[36] H. B. Hartanto, B. Jäger, L. Reina, and D. Wackeroth, Phys.Rev., **D91**, 094003 (2015), arXiv:1501.04498 [hep-ph].
[37] The Higgs Cross Section Working Group, `https://cern.ch/twiki/bin/view/LHCPhysics/LHCHXSWG`.
[38] K. A. Olive *et al.* (Particle Data Group), Chin. Phys., **C38**, 090001 (2014).
[39] J. Butterworth *et al.*, J. Phys., **G43**, 023001 (2016), arXiv:1510.03865 [hep-ph].
[40] A. Buckley, J. Ferrando, S. Lloyd, K. Nordström, B. Page, M. Rüfenacht, M. Schönherr, and G. Watt, Eur. Phys. J., **C75**, 132 (2015), arXiv:1412.7420 [hep-ph].
[41] S. Dulat, T. J. Hou, J. Gao, M. Guzzi, J. Huston, P. Nadolsky, J. Pumplin, C. Schmidt, D. Stump, and C. P. Yuan, (2015), arXiv:1506.07443 [hep-ph].
[42] L. A. Harland-Lang, A. D. Martin, P. Motylinski, and R. S. Thorne, Eur. Phys. J., **C75**, 204 (2015), arXiv:1412.3989 [hep-ph].
[43] R. D. Ball *et al.* (NNPDF), JHEP, **04**, 040 (2015), arXiv:1410.8849 [hep-ph].
[44] M. Cacciari and G. P. Salam, Phys. Lett., **B641**, 57 (2006), arXiv:hep-ph/0512210 [hep-ph].
[45] M. Cacciari, G. P. Salam, and G. Soyez, Eur. Phys. J., **C72**, 1896 (2012), arXiv:1111.6097 [hep-ph].
[46] It does not account for e.g. the opening of new partonic channels at higher orders.
[47] G. Watt and R. S. Thorne, JHEP, **08**, 052 (2012), arXiv:1205.4024 [hep-ph].
[48] J. Gao and P. Nadolsky, JHEP, **07**, 035 (2014), arXiv:1401.0013 [hep-ph].
[49] S. Carrazza, S. Forte, Z. Kassabov, J. I. Latorre, and J. Rojo, Eur. Phys. J., **C75**, 369 (2015), arXiv:1505.06736 [hep-ph].
[50] S. Dittmaier *et al.* (LHC Higgs Cross Section Working Group), (2011), doi:10.5170/CERN-2011-002, arXiv:1101.0593 [hep-ph].